Title

Detection of Bacteria-Specific Metabolism Using Hyperpolarized [2-13C]Pyruvate

Journal

ACS Infectious Diseases, 4(5)

ISSN

2373-8227

Authors

Sriram, Renuka

Sun, Jinny

Villanueva-Meyer, Javier

et al.

Publication Date

2018-05-11

DOI

10.1021/acsinfecdis.7b00234

Peer reviewed

HHS Public Access

Author manuscript

ACS Infect Dis. Author manuscript; available in PMC 2018 June 20.

Published in final edited form as:

ACS Infect Dis. 2018 May 11; 4(5): 797–805. doi:10.1021/acsinfecdis.7b00234.

Detection of bacteria-specific metabolism using hyperpolarized [2-^{13}C] pyruvate

Renuka Sriram[1], **Jinny Sun**[1], **Javier Villanueva-Meyer**[1], **Christopher Mutch**[1], **Justin De Los Santos**[1], **Jason Peters**[2], **David E. Korenchan**[1], **Kiel Neumann**[3], **Mark Van Criekinge**[1], **John Kurhanewicz**[1], **Oren Rosenberg**[4,*], **David Wilson**[1,*], and **Michael A. Ohliger**[1,5,*]

[1]Radiology and Biomedical Imaging, University of California San Francisco, San Francisco, CA, USA. Department of Radiology and Biomedical Imaging, University of California, San Francisco, 1600 4th St, Box 2520, San Francisco CA 94158

[2]Microbiology and Immunology, University of California, San Francisco, California, USA. 600 16th Street, San Francisco CA 94158

[3]Department of Radiology, University of Virginia, Charlottesville, Virginia, USA. 480 Ray C. Hunt Dr. Charlottesville, VA 22903

[4]Division of Infectious Diseases, School of Medicine, University of California, San Francisco, California, USA. 505 Parnassus Ave., San Francisco, CA 94143, USA

[5]Zuckerberg San Francisco General Hospital, San Francisco, CA USA. 1001 Potrero Ave., San Francisco, CA 94110

Abstract

The differentiation of bacterial infection from other causes of inflammation is difficult in clinical practice and is critical where patient outcomes rely heavily on early interventions. In addition to physical exam and laboratory markers, several imaging modalities are frequently employed, but these techniques generally target the host immune response, rather than the living microorganisms themselves. Here, we describe a method to detect bacteria-specific metabolism using hyperpolarized (HP) ^{13}C magnetic resonance spectroscopy. This technology allows visualization of the real-time conversion of enriched ^{13}C substrates to their metabolic products, identified by their distinct chemical shifts. We have identified the rapid metabolism of HP [2-^{13}C]pyruvate to [1-^{13}C]acetate as a metabolic signature of common bacterial pathogens. We demonstrate this conversion in representative Gram negative and Gram positive bacteria, namely *Escherichia coli* and *Staphylococcus aureus*, and its absence in key mammalian cell-types. Furthermore this

*Correspondence and Reprint Request: Michael Ohliger, M.D., Ph.D., michael.ohliger@ucsf.edu. David Wilson, M.D., Ph.D., david.m.wilson@ucsf.edu. Oren Rosenberg, M.D., Ph.D., oren.rosenberg@ucsf.edu.

Conflicts of interest

The authors declare that they have no conflicts of interest with the contents of this article.

Author contributions

RS, JS, JV-M, CM, KN prepared the bacterial culture for the NMR experiments
RS, JS, JDS, JV-M, CM and MVC helped with the bioreactor optimization and execution.
JP, OR provided microbiology expertise
DEK, DW, RS, JS, MO helped with the hyperpolarized preparation of the probes
RS, MO, DW, JK, OR were involved in the experimental design, data analysis and interpretation and manuscript preparation
All the authors aided in revising the article critically for important intellectual content and approved the final version.

conversion was successfully modulated in three mutant strains, corresponding to deletions of relevant enzymes.

Graphical Abstract

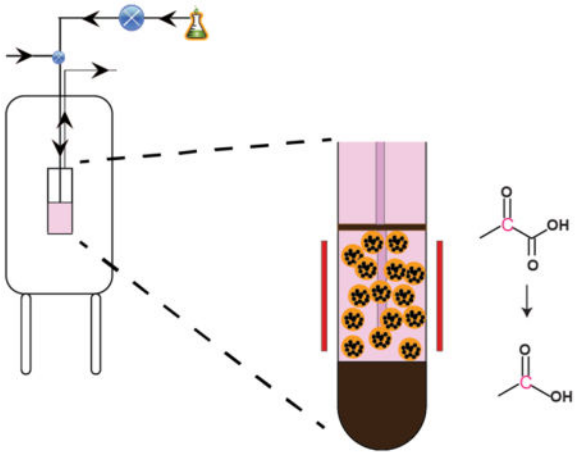

Keywords

Hyperpolarized ^{13}C nuclear magnetic resonance (MR); dynamic nuclear polarization (DNP); pyruvate; acetate; bacterial metabolism

Distinguishing bacterial infections from non-infectious mimics is an important clinical challenge. Laboratory markers such as erythrocyte sedimentation rate or the C-reactive protein are sensitive to systemic inflammation and are therefore not specific for infection. Standard morphologic imaging modalities such as computed tomography (CT) and magnetic resonance imaging (MRI) are similarly non-specific. For example, an active spine infection may look similar on MRI to other pathologies including age-related degeneration [1]. In patients with severe pancreatitis or postoperative fever, infected fluid collections (that must be drained) cannot be differentiated from sterile inflammation using CT or MRI [2–4] and the morbidity of intervention in the case of a false positive can be very high.

Current nuclear-medicine based molecular imaging approaches also have significant limitations in the accurate diagnosis of infection. For example, common clinical tools, such as single photon emission computed tomography (SPECT) ^{111}In white blood cell scanning [5] and gallium scintigraphy target the inflammatory response to infection and do not detect the organisms themselves. Full-body positron emission tomography (PET) using ^{18}F-fluorodeoxyglucose (FDG) has recently been used in the workup for fever of unknown origin [6], to detect the upregulated glycolysis characteristic of activated immune cells. However, like SPECT approaches, FDG-PET detects the host immune response rather than the living bacteria. Thus, new diagnostic tools are required to directly detect bacteria in infected tissues.

Several novel approaches to imaging infection have recently been described that overcome the challenges faced by conventional approaches, by targeting metabolic pathways that are

unique to bacteria. For example, gram-negative bacteria are able to use sorbitol as a metabolic substrate, while mammalian cells cannot. Based on this difference, ^{18}F-deoxysorbitol (^{18}F-FDS) has been developed as a PET-based marker of infection and has been used to distinguish infectious myositis from sterile inflammation in a mouse model [7]. Similarly, we have recently described the use of D-[methyl-^{11}C]methionine to image bacterial infection *in vivo*, based on the selective incorporation of D-amino acids into the bacterial cell wall [8,9].

Recently, a metabolic technology has emerged to complement PET that is particularly sensitive to divergent metabolism, namely hyperpolarized magnetic resonance (HP MR). HP MR is a powerful tool for the molecular imaging of metabolism. This methodology is based on polarizing nuclear spins in an amorphous solid state at ~1.2°K through coupling of the nuclear spins with unpaired electrons provided via an organic free radical. ^{13}C labeled substrates have been recently polarized to obtain dramatic enhancements of the ^{13}C MR signals (>50,000 fold at 3T) of the substrate as well as subsequent metabolic products [10]. HP ^{13}C MR has been applied to preclinical animal models of cancer [11], cardiac disease [12], and diabetes [13]. HP ^{13}C pyruvate MR has already been translated to human imaging for cancer applications [14], and numerous clinical trials are ongoing. HP ^{13}C MR-based strategies for imaging infection have great potential for several reasons: 1) HP ^{13}C MR does not require ionizing radiation, making it ideal for use in vulnerable populations including children, 2) HP ^{13}C MR can distinguish between the injected tracer and bacteria-specific downstream metabolites with exceptionally high specificity, and 3) chemical shift separation of HP metabolites allows multiple agents to be imaged simultaneously [15], probing different metabolic pathways.

In this study, we demonstrate the rapid metabolism of [2-^{13}C]pyruvate into HP [1-^{13}C]acetate in two common species of pathogenic bacteria, namely *E. coli* and *S. aureus*. This conversion is contrasted with [2-^{13}C]pyruvate metabolism in mammalian cell lines. Finally, we employ an MR-compatible perfusion cell culture system (also known as a bioreactor) to investigate the mechanism of HP [1-^{13}C]acetate generation in *E. coli*.

RESULTS

E. coli suspensions probed with HP ^{13}C pyruvate revealed [1-^{13}C]acetate and ^{13}C formate resonances as potential bacteria-specific signals

We performed initial studies using HP ^{13}C pyruvate in *E. coli* cell suspensions to identify promising bacteria-specific metabolite signals. A mixture of HP [1-^{13}C]pyruvate and HP [2-^{13}C]pyruvate was introduced into small-volume cultures and examined at high-field (11.7 T) by ^{13}C NMR. Both isotopomers of pyruvate were used in this initial experiment so that we could simultaneously explore multiple metabolic pathways in bacteria and mammalian cells. Using a mixture of [1-^{13}C] and [2-^{13}C]pyruvic acid, rather than doubly-labeled [1,2-^{13}C]pyruvate, permitted us to minimize the spectral complexity and associated relaxation mechanisms resulting from carbon-carbon coupling in the doubly labeled compound.

HP [1-^{13}C]pyruvate and HP [2-^{13}C]pyruvate were metabolized by *E. coli* to produce formate and acetate, respectively (Figure 1A). The intermediates acetyl-coA, carbon dioxide, and bicarbonate were also observed (Figure 1B). Based on these initial results, we identified hyperpolarized [1-^{13}C]acetate (average signal-to-noise ratio of 51± 28, acetate/pyruvate ratio 0.04 ± 0.007, N=5) as a promising bacteria-specific resonance. This peak assignment to acetate was also confirmed using thermal ^{1}H NMR measurements (see supplementary figure S1). Formate, produced from pyruvate via the enzyme pyruvate-formate lyase, was another potentially specific bacterial product, but had insufficient chemical shift difference (0.74 ppm) from [1-^{13}C]pyruvate for detailed study in biological systems. *S. aureus*, an important Gram-positive pathogen, also exhibited acetate conversion from pyruvate. When *S. aureus* cultures were combined with hyperpolarized [2-^{13}C]pyruvate, [1-^{13}C]acetate was seen as a metabolic product (Figure 2). The ratio of the acetate to pyruvate resonances was 0.016 ± 0.007 (N=3), similar to that seen in *E. coli* cells.

An NMR-compatible, perfused bioreactor provides a platform for rigorous study of [2-^{13}C] pyruvate metabolism in bacteria

Based on these encouraging results, we optimized a 3D culture platform to address some of the limitations encountered studying bacterial metabolism in small-volume cell-suspensions via NMR. Simple experiments in an NMR tube make quantification difficult for two reasons: First, because the cells settle to the bottom of the NMR tube during data acquisition, it is difficult to quantify the number of cells contributing to ^{13}C signal in the sensitive volume of the NMR receiver coil. This settling also causes inhomogeneity that degrades the signal intensity. Second, it is difficult to maintain the consistent environment necessary for extended and repeated experiments due to lack of oxygen and fresh nutrient supply. We therefore optimized an NMR-compatible cell culture bioreactor for bacteria experiments, which permitted reproducible, quantitative measurements of hyperpolarized signals and enzyme kinetics. Our NMR-compatible 3D cell and tissue culture bioreactor was based on a design that we have previously developed for mammalian cells and tissues [16–18] (see supplementary figure S2 for schematic). To confirm that encapsulated bacteria could be kept in a stable metabolic state over the course of several experiments, we studied the bioenergetics of *E. coli* using phosphorus (^{31}P) NMR (Figure 3A). ^{31}P NMR visible nucleoside triphosphate (NTP) peaks are predominantly comprised of adenosine triphosphate (ATP) [19] and are often used to assess the viability of cells and tissues. The adenylate energy charge was calculated to be 0.75, indicating viable cells[20]. Stable nucleoside triphosphate (NTP) peaks were observed in *E. coli* for 2 hours (see supplementary figure S3), which was the maximal duration of the HP NMR bioreactor experiments per biological replicate. Therefore, bacteria could be kept in a steady metabolic state during the experiment.

Figure 3B demonstrates the dynamic HP ^{13}C spectra of *E. coli* encapsulated in alginate microspheres upon infusion of HP [2-^{13}C]pyruvate with a temporal resolution of 3 seconds. The rise and fall of the acetate signal arising from the conversion of [2-^{13}C]pyruvate by the *E. coli* cells represents the initial production rate and the subsequent washout of the signal due to the longitudinal relaxation of the hyperpolarized signal. The summed spectrum at the

very end of the series is illustrative of the total signal of each of the metabolites for the entire time course (~ 2.5 minutes).

[1-^{13}C] acetate is a product of HP [2-^{13}C]pyruvate metabolism in *E. coli* but not in cancer or activated immune cells

To demonstrate that the HP acetate signal observed was unique to bacteria, we compared the metabolism of HP pyruvate in an *E. coli*-loaded bioreactor to the metabolism seen in representative malignant and inflammatory mammalian cells, namely renal cell cancer (UOK 262) and activated macrophages (RAW 264.7). Equal amounts of HP [1-^{13}C] pyruvate and HP [2-^{13}C] pyruvate mixture were polarized and injected into the mammalian and bacterial cells under study. We detected hyperpolarized acetate peaks in *E. coli* but not in mammalian cells (Figure 4). In contrast, spectra derived from both renal cell carcinoma cells and activated macrophages demonstrated production of [1-^{13}C]lactate from [1-^{13}C] pyruvate, which is expected due to upregulated oxidative glycolysis in these cells [21,22].

Mutant *E. coli* strains studied with HP [2-^{13}C]pyruvate show multiple compensatory pathways of acetate production

We further interrogated the multiple pathways of acetate production that exist in bacteria using *E. coli* strains for which key metabolic enzymes have been deleted, namely *pta, ackA* and *poxB* (Figure 5A); these enzymes make up crucial pathways for acetate production. Spectra were obtained using our NMR-compatible bioreactor system following injection of [2-^{13}C]pyruvate into each *E. coli* mutant as well as the wild type (Figure 5B). Using our hyperpolarized ^{13}C MR technique, it was possible to observe the high energy intermediate, acetyl phosphate (acetyl-PO_4), of the *pta/ackA* pathway. The chemical shift reference of this intermediate was confirmed using external standard measurements of acetate and acetyl-PO_4 (supplementary figure S4). The Δ*pta* strain produced high levels of acetate and low levels of acetyl-PO_4, while the Δ*ackA* strain had drastically reduced levels of acetate, with a corresponding buildup of acetyl-PO_4 and acetyl-CoA (representative spectra shown in Figure 5B). Finally, the Δ*poxB* strain had lower acetate production and no detectable signals from the intermediates (acetyl-PO_4 and acetyl-CoA).

The dynamic traces of the signals obtained from the bioreactor experiments were further quantified by integrating the peak areas of each metabolite for the entire time course, and the mean and standard deviation were computed (Figure 5C) and normalized to the pyruvate signal. The acetate/pyruvate ratios were significantly reduced ($p<0.05$) in the Δ*ackA* (0.0016 ± 0.0005) and Δ*pta* strains (0.0032 ± 0.0014) when compared to the wildtype cells (0.0069 ± 0.0006). While the *pta* knockout cells had slightly higher acetate/pyruvate ratios (0.011 ± 0.001) compared to wildtype, these ratios were not statistically significant. Acetyl-coA signal was observed robustly in the Δ*ackA* strain, indicating the relatively higher pool size of this metabolic intermediate consistent with a truncation of the *pta/ackA* pathway. However, Δ*pta* and Δ*ackA* strains both accumulated the high energy signaling molecule, acetyl-PO_4, further reinforcing the dysfunctional *pta/ackA* pathway. The Δ*ackA* strain had significantly ($p<0.05$) higher acetyl-phosphate/pyruvate ratio (0.014 ± 0.008) compared to Δ*pta* strain (0.004 ± 0.001). Interestingly, this disrupted pathway resulted in the increased lactate signal,

with the Δ*ackA* strain having a slightly higher lactate/pyruvate ratio (0.0067 ± 0.0034) compared to the Δ*pta* strain (0.0026 ± 0.001).

Discussion

In this study, we demonstrated robust production of HP [1-^{13}C] acetate from HP [2-^{13}C]pyruvate in two common pathogenic strains of bacteria – *E. coli* and *S. aureus* – but not in mammalian cell lines. Specifically, UOK262 renal cell cancer cell lines and activated macrophages were studied because both tumors and inflammatory cells are important infection mimics in clinical practice. These results suggest that HP [1-^{13}C] acetate is a potential specific marker of bacterial cells and may in the future aid in distinguishing infections from non-infectious processes in the body.

Pyruvate is a key intermediate in energy metabolism and is used by both bacteria and mammalian cells. In bacteria, pyruvate is used to generate acetate, as a mechanism for recycling NAD+ and coenzyme A, particularly in states of glucose (carbon) excess [23]. Bacterial-derived acetate is predominantly produced through acetyl-CoA through a reaction catalyzed by the enzymes Pta and AckA, (Figs 1A and 5A). This pathway is key for generating ATP essential for the anaerobic growth of *E. coli* [24]. Although mammalian cells have the capacity to produce acetate from pyruvate, acetate is produced much more slowly by mammalian cells. The rate of acetate production in mammalian cells is approximately 0.18 μmol acetate/h/mmol of glucose/100g of protein [25]. By contrast, wild type *E. coli* in culture produce approximately 46562 μmol acetate/h/mmol glucose/100g of protein [26]. The dramatically decreased production of acetate observed in mammalian cells (> 10^5 slower rate) has been attributed to a tightly regulated acetyl-CoA pool [27]. Furthermore, in mammalian cells, acetyl-CoA is compartmentalized in mitochondria, impacting the rate of acetate production. In order to produce acetate, acetyl-CoA formed from pyruvate in the mitochondria needs to be transported back to the cytosol and hydrolyzed via acetyl-CoA hydrolase. However, this transport requires the citrate/malate shuttle to transfer acetyl group equivalents from the mitochondria to the cytosol across the acetyl-CoA-impermeable mitochondrial inner membrane [28]. The multiple steps involved in eukaryotic acetate formation from pyruvate should prevent visualization of this conversion within HP signal lifetimes as is observed in this study.

In addition to comparing acetate production between bacteria and mammalian cells, we were able to confirm the pathway of acetate production in *E. coli* to be as shown in figure 5A by demonstrating decreased acetate production with key enzyme knockouts. The Δ*ackA* strain had the lowest acetate production, which is consistent with prior results using different techniques [29,30]. Although acetyl-coA was only observed in the Δ*ackA* knockouts robustly, its absence in the wild type and Δ*pta* is a consequence of decreased number of cells and reduced apparent pyruvate resident time in the active region of the coil of the bioreactor set-up and not of the enzyme knockouts itself. We have shown, for the first time, the real-time measurement of the high energy signaling molecule acetyl-phosphate using hyperpolarized magnetic resonance spectroscopy. This intermediate metabolite was appropriately observed only in the Δ*pta* and Δ*ackA* strains. The enzyme knockouts that we studied are the only enzymes known to produce acetyl-PO_4 in *E. coli* [31]. The presence of acetyl-PO_4 in the Δ*pta*

mutant could be indicative of alternative metabolic pathways that evade the requirement for *pta* enzyme or the reversible flux of the ackA enzyme, which needs to be verified by steady state metabolite analysis. These observations show that the bioreactor platform can be a powerful tool to interrogate the rate-limiting steps and key metabolic intermediates of these pathways. The Δ*pta* strain also produced increased acetate signal compared to the wild type cells, presumably due to a compensatory mechanism via the *poxB* pathway. Furthermore with the disruption of the *pta*/*ackA* pathway, the pyruvate flux to lactate is increased, which is also consistent with previous non-HP studies [32]. This *pta*/*ackA* pathway has also been shown to be critical for *S. aureus* survival [33]. Although the specific mechanism has remained elusive, the *pta/ackA* pathway has been shown to be essential in several microbes for colonization of hosts [34]. Furthermore, this pathway has been shown to have a deleterious effect on protein folding and aggregation resulting in temperature sensitive attenuated growth rate [35]. All of these taken together reinforce the central role of acetate in bacterial metabolism thereby making for a robust biomarker.

Bacterial metabolism has been previously investigated using HP ^{13}C glucose in *E. coli* [36]. In that study, the common fermentative byproduct, ethanol, was observed. In contrast, we did not observe ethanol production, which is likely due to the short T_1 of ethanol compared with the longer repetition time used in our study (3 seconds). The use of HP [2-^{13}C]pyruvate to study infection is advantageous compared to HP ^{13}C glucose because HP [1-^{13}C]pyruvate is already being used for clinical studies in humans with cancer [14]. Therefore, HP [2-^{13}C]pyruvate is expected to have a low barrier to eventual clinical translation.

Our study has several limitations, but the results presented here are promising and warrant further investigation in animal models. We demonstrate clear metabolic signatures within bacterial and mammalian cell lines, but further studies in animals are required to demonstrate that the technique is sensitive enough to detect bacterial metabolism of infections *in vivo*. Very little is known about the number of bacteria within an active infection; one estimate is 2×10^8 colony-forming units (CFUs)/mL [37], which is on the same order of magnitude as the bioreactor-loaded cells in our study. While the *in vivo* sensitivity of this methodology is unknown at this stage, the inherent enhancement of the hyperpolarization technique (up to 10^6 versus thermal MRI) is a huge advantage over other detection schemes. Furthermore, one potential confounding factor for *in vivo* application could be the very close resonance (0.15 ppm upfield) of [5-^{13}C]glutamate to that of the [1-^{13}C] acetate peak both produced from metabolism from [2-^{13}C]pyruvate. Although, we have shown in this work conclusively that the peak we observe is that of acetate (via thermal labeling and enzyme knockout measurements), this would need careful evaluation for *in vivo* applications. We also showed specific bacterial metabolism compared to two important mammalian cell lines, but this may not be representative of other cell types that may be encountered *in vivo*. However, our work is consistent with *in vitro* studies of other bacterial species, such as *Shigella,* have shown similar increased acetate production as a consequence of infection [38].

In conclusion, metabolism of HP [2-^{13}C]pyruvate may represent a way to distinguish living bacteria from non-infectious mimics such as cancer and sterile inflammation. Further *in vivo*

studies are warranted to determine if this technique has enough sensitivity to detect infections.

Methods

Bacterial Strains and deletion mutants

Wild-type strains—All *E. coli* used in this study were a kind gift from the laboratory of Dr. Carol Gross (Department of Microbiology and Immunology at University of California, San Francisco). The wild type *E. coli* used in this study was the K-12 BW25113 strain. The *S. aureus* was purchased from ATCC (ATCC 12600). *E. coli mutants*: In order to interrogate individual pathways involved in acetate production, deletion mutants were obtained from the Keio collection [39]. Specifically, 3 deletion strains were examined: 1) deletion of phospho-transacetylase (*pta*), which converts acetyl-CoA to acetyl-phosphate, 2) deletion of acetate kinase (*ackA*) which converts acetyl phosphate to acetate and 3) deletion of pyruvate dehydrogenase *poxB*, a flavoprotein that can convert pyruvate to acetate in a single step.

E. coli and S. aureus liquid cultures

Two types of cell preparations were used for NMR experiments. Initial experiments were performed using simple liquid cultures (“cell slurries”) placed in NMR tubes. Further experiments were performed using an NMR-compatible bioreactor (described below) that allowed finer control of the cell environment during the experiment. For experiments involving simple liquid cultures, *E. coli* and *S. aureus* were inoculated in 20 ml lysogeny broth (LB) medium from agar plates and were grown overnight at 37° C in shake flask cultures and grown to OD_{600} of 0.6 to 0.8. Centrifuged cell pellets were resuspended in 500 μl of 40 mM HEPES buffer at pH 7.3 for HP ^{13}C NMR experiments.

Bioreactor setup and encapsulation of cells

E. coli cells, both wild-type and mutants were inoculated in 50 ml LB medium from an agar plate and grown to OD_{600} of 0.6 – 0.8 before being spun down for encapsulation in alginate at a density of 1×10^9 cells/ml using techniques to those previously described [16]. A renal cell carcinoma cell line, UOK262, was used as a representative cancer cell line (cells obtained from Dr. W. Marston Linehan, National Cancer Institute, Bethesda, MD. Cells and authenticated using STR profiling, October 2012). The UOK262 cells were also encapsulated in alginate microspheres identical to prior publications [40] from our group. To model the inflammatory response, a mouse macrophage cell line, J774A.1, was obtained from ATCC. These cells were grown on the surface of microcarrier beads (Cytodex®, Sigma Aldrich, St. Louis, MO, USA) as these substrates were found to be optimal for cell proliferation and metabolism. To mimic the activated state of macrophages, the cells were stimulated using lipopolysaccharideat 50 ng/ml for 24 hours derived from *E. coli* (Sigma Aldrich, St. Louis, MO, USA).

Once the cells were prepared for the bioreactor experiments with alginate or microcarrier beads, as described above, 250 μl of the cell-laden spheres were loaded into the 5 mm bioreactor. The cells were continuously perfused with high glucose (25 mM) DMEM media

warmed to 37 °C and provided with 95% oxygen at 1 ml/min flow rate as described previously [18].

Preparation and polarization of ^{13}C enriched samples

Samples of enriched and concentrated [1-^{13}C] and [2-^{13}C]pyruvic acid were prepared for dynamic nuclear polarization (DNP) as detailed in prior work [15]. For cell suspension experiments, a mixture of [1-^{13}C] and [2-^{13}C]pyruvic acid was used. This mixture was polarized using a 3 T Hypersense (Oxford Instruments) DNP and dissolved in a phosphate buffer. Approximately 16 μmols of co-polarized [1-^{13}C]pyruvate and [2-^{13}C]pyruvate [15] dissolution solutions were added to the cells. For subsequent experiments using the bioreactor platform (wild type *E. coli* and variants), bacteria in the bioreactor were injected with 8 μmols of [2-^{13}C]pyruvate alone.

NMR Experiments

All hyperpolarized experiments were conducted using a 11.7 Tesla Varian INOVA (Agilent Technologies, Santa Clara, Ca, USA) NMR spectrometer. For the bacterial cell suspensions, 500 μl of the dissolution solution was quickly added to the 500 μl of cells resuspended in HEPES buffer, rapidly mixed and inserted into the magnet. For the bioreactors, the dissolution solution was injected under flow continuously for 90 seconds at 0.5 ml/min. NMR data were acquired every 3 s using a dynamic pulse-acquire sequence and 30° RF pulses, for a total of for 300 s, with a spectral bandwidth of 20 KHz and 40000 points.

For bioreactor studies, ^{31}P spectra was also acquired to ensure viability as previously described [18]. Briefly, data was acquired with a spectral badnwith of 12 KHz, 2048 averages and 1s acquisition time using a pulse-acquire sequence employing a 90° RF pulse. The chemical shift was referenced to α-NTP peak at −10 ppm as seen in prior bacterial work [41,42].

Data Analysis

Dynamic spectra were summed and all analyses were performed using MNOVA (Mestrelab Research, Spain). All results are reported as mean ± standard deviation. Chemical shift assignments were made based on literature [36] and databases (University of Texas, Southwestern, Advanced Imaging Research Center, http://www.utsouthwestern.edu/education/medical-school/departments/airc/tools-references/chemical-shifts/andHumanmetabolomedatabase,hmdb.ca). Statistical significance was determined using Student's T-test with a threshold of significance denoted by $p < 0.05$.

Supplementary Material

Refer to Web version on PubMed Central for supplementary material.

Acknowledgments

We would like to acknowledge grant funding from: National Institutes of Health (P41 EB013598, RO1 EB024014), Department of Defense (USAMRMC CA110032) and Research Evaluation and Allocation Committee Award and Department of Radiology and Biomedical Imaging Seed Grant, University of California, San Francisco.

References

1. Baker JC, Demertzis JL, Rhodes NG, Wessell DE, Rubin DA. Diabetic musculoskeletal complications and their imaging mimics. Radiographics. 2012; 32(7):1959–1974. DOI: 10.1148/rg.327125054 [PubMed: 23150851]
2. Segal D, Mortele KJ, Banks PA, Silverman SG. Acute necrotizing pancreatitis: role of CT-guided percutaneous catheter drainage. Abdom Imaging. 2007; 32(3):351–361. DOI: 10.1007/s00261-007-9221-5 [PubMed: 17502982]
3. Shyu JY, Sainani NI, Sahni VA, Chick JF, Chauhan NR, Conwell DL, Clancy TE, Banks PA, Silverman SG. Necrotizing Pancreatitis: Diagnosis, Imaging, and Intervention. Radiographics. 2014; 34(5):1218–1239. DOI: 10.1148/rg.345130012 [PubMed: 25208277]
4. Maher MM, Lucey BC, Gervais DA, Mueller PR. Acute pancreatitis: the role of imaging and interventional radiology. Cardiovascular and interventional radiology. 2004; 27(3):208–225. DOI: 10.1007/s00270-003-1907-7 [PubMed: 15024494]
5. Lewis SS, Cox GM, Stout JE. Clinical Utility of Indium 111-Labeled White Blood Cell Scintigraphy for Evaluation of Suspected Infection. Open Forum Infectious Diseases. 2014; 1(2):ofu089–ofu089. DOI: 10.1093/ofid/ofu089 [PubMed: 25734155]
6. Gafter-Gvili A, Raibman S, Grossman A, Avni T, Paul M, Leibovici L, Tadmor B, Groshar D, Bernstine H. [18F]FDG-PET/CT for the diagnosis of patients with fever of unknown origin. QJM. 2015; 108(4):289–298. DOI: 10.1093/qjmed/hcu193 [PubMed: 25208896]
7. Weinstein EA, Ordonez AA, DeMarco VP, Murawski AM, Pokkali S, MacDonald EM, Klunk M, Mease RC, Pomper MG, Jain SK. Imaging Enterobacteriaceae infection in vivo with 18F-fluorodeoxysorbitol positron emission tomography. Sci Transl Med. 2014; 6(259):259ra146–259ra146. DOI: 10.1126/scitranslmed.3009815
8. Neumann KD, Villanueva-Meyer JE, Mutch CA, Flavell RR, Blecha JE, Kwak T, Sriram R, VanBrocklin HF, Rosenberg OS, Ohliger MA, et al. Imaging Active Infection in vivo Using D-Amino Acid Derived PET Radiotracers. Scientific Reports. 2017; 7(1):7903.doi: 10.1038/s41598-017-08415-x [PubMed: 28801560]
9. Sellmyer MA, Lee I, Hou C, Weng C-C, Li S, Lieberman BP, Zeng C, Mankoff DA, Mach RH. Bacterial infection imaging with [18F]fluoropropyl-trimethoprim. Proc Natl Acad Sci USA. 2017; 114(31):8372–8377. DOI: 10.1073/pnas.1703109114 [PubMed: 28716936]
10. Ardenkjaer-Larsen JH, Fridlund B, Gram A, Hansson G, Hansson L, Lerche MH, Servin R, Thaning M, Golman K. Increase in signal-to-noise ratio of > 10,000 times in liquid-state NMR. Proc Natl Acad Sci USA. 2003; 100(18):10158–10163. DOI: 10.1073/pnas.1733835100 [PubMed: 12930897]
11. Kurhanewicz J, Vigneron DB, Brindle K, Chekmenev EY, Comment A, Cunningham CH, DeBerardinis RJ, Green GG, Leach MO, Rajan SS, et al. Analysis of cancer metabolism by imaging hyperpolarized nuclei: prospects for translation to clinical research. Neoplasia. 2011; 13(2):81–97. DOI: 10.1593/neo.101102 [PubMed: 21403835]
12. Schroeder MA, Lau AZ, Chen AP, Gu Y, Nagendran J, Barry J, Hu X, Dyck JRB, Tyler DJ, Clarke K, et al. Hyperpolarized (13)C magnetic resonance reveals early- and late-onset changes to in vivo pyruvate metabolism in the failing heart. Eur J Heart Fail. 2013; 15(2):130–140. DOI: 10.1093/eurjhf/hfs192 [PubMed: 23258802]
13. Lee P, Leong W, Tan T, Lim M, Han W, Radda GK. In Vivo hyperpolarized carbon-13 magnetic resonance spectroscopy reveals increased pyruvate carboxylase flux in an insulin-resistant mouse model. Hepatology. 2013; 57(2):515–524. DOI: 10.1002/hep.26028 [PubMed: 22911492]
14. Nelson SJ, Kurhanewicz J, Vigneron DB, Larson PEZ, Harzstark AL, Ferrone M, Van Criekinge M, Chang JW, Bok R, Park I, et al. Metabolic Imaging of Patients with Prostate Cancer Using Hyperpolarized [1-13C]Pyruvate. Sci Transl Med. 2013; 5(198):198ra108.doi: 10.1126/scitranslmed.3006070
15. Wilson DM, Keshari KR, Larson PEZ, Chen AP, Hu S, Van Criekinge M, Bok R, Nelson SJ, Macdonald JM, Vigneron DB, et al. Multi-compound polarization by DNP allows simultaneous assessment of multiple enzymatic activities in vivo. J Magn Reson. 2010; 205(1):141–147. DOI: 10.1016/j.jmr.2010.04.012 [PubMed: 20478721]

16. Sriram R, Van Criekinge M, Hansen A, Wang ZJ, Vigneron DB, Wilson DM, Keshari KR, Kurhanewicz J. Real-time measurement of hyperpolarized lactate production and efflux as a biomarker of tumor aggressiveness in an MR compatible 3D cell culture bioreactor. NMR Biomed. 2015; 28(9):1141–1149. DOI: 10.1002/nbm.3354 [PubMed: 26202449]
17. Sriram R, Van Criekinge M, DeLos Santos J, Keshari KR, Peehl DM, Wang ZJ. Non-Invasive Differentiation of Benign Renal Tumors from Clear Cell Renal Cell Carcinomas Using Clinically Translatable Hyperpolarized 13C Pyruvate Magnetic Resonance. Tomography. 2016; 2(1):35–42. DOI: 10.18383/j.tom.2016.00106 [PubMed: 27227168]
18. Keshari KR, Wilson DM, Van Criekinge M, Sriram R, Koelsch BL, Wang ZJ, VanBrocklin HF, Peehl DM, O'Brien T, Sampath D, et al. Metabolic response of prostate cancer to nicotinamide phophoribosyltransferase inhibition in a hyperpolarized MR/PET compatible bioreactor. Prostate. 2015; 75(14):1601–1609. DOI: 10.1002/pros.23036 [PubMed: 26177608]
19. Bak MI, Ingwall JS. NMR-invisible ATP in heart: fact or fiction? Am J Physiol. 1992; 262(6 Pt 1):E943–E947. DOI: 10.1152/ajpendo.1992.262.6.E943 [PubMed: 1616027]
20. Chapman AG, Fall L, Atkinson DE. Adenylate Energy Charge in Escherichia-Coli During Growth and Starvation. J Bacteriol. 1971; 108(3):1072. [PubMed: 4333317]
21. Warburg O. The Metabolism of Carcinoma Cells. The Journal of Cancer Research. 1925; 9(1):148–163. DOI: 10.1158/jcr.1925.148
22. O'Neill LAJ, Kishton RJ, Rathmell J. A guide to immunometabolism for immunologists. Nat Rev Immunol. 2016; 16(9):553–565. DOI: 10.1038/nri.2016.70 [PubMed: 27396447]
23. Wolfe AJ. The acetate switch. Microbiol Mol Biol Rev. 2005; 69(1):12–50. DOI: 10.1128/MMBR.69.1.12-50.2005 [PubMed: 15755952]
24. Hasona A, Kim Y, Healy FG, Ingram LO, Shanmugam KT. Pyruvate Formate Lyase and Acetate Kinase Are Essential for Anaerobic Growth of Escherichia coli on Xylose. J Bacteriol. 2004; 186(22):7593–7600. DOI: 10.1128/JB.186.22.7593-7600.2004 [PubMed: 15516572]
25. Rae C, Fekete AD, Kashem MA, Nasrallah FA, Bröer S. Metabolism, compartmentation, transport and production of acetate in the cortical brain tissue slice. Neurochem Res. 2012; 37(11):2541–2553. DOI: 10.1007/s11064-012-0847-5 [PubMed: 22851350]
26. Contiero J, Beatty C, Kumari S, DeSanti CL, Strohl WR, Wolfe A. Effects of mutations in acetate metabolism on high-cell-density growth of Escherichia coli. Journal of Industrial Microbiology and Biotechnology. 2000; 24(6):421–430. DOI: 10.1038/sj.jim.7000014
27. Choudhary C, Weinert BT, Nishida Y, Verdin E, Mann M. The growing landscape of lysine acetylation links metabolism and cell signalling. Nature Reviews Molecular Cell Biology. 2014; 15(8):536–550. DOI: 10.1038/nrm3841 [PubMed: 25053359]
28. Hatzivassiliou G, Zhao F, Bauer DE, Andreadis C, Shaw AN, Dhanak D, Hingorani SR, Tuveson DA, Thompson CB. ATP citrate lyase inhibition can suppress tumor cell growth. Cancer Cell. 2005; 8(4):311–321. DOI: 10.1016/j.ccr.2005.09.008 [PubMed: 16226706]
29. Enjalbert B, Millard P, Dinclaux M, Portais JC, Letisse F. Acetate fluxes in Escherichia coli are determined by the thermodynamic control of the Pta-AckA pathway. Scientific Reports. 2017; 7:42135.doi: 10.1038/srep42135 [PubMed: 28186174]
30. Wolfe AJ. The acetate switch. Microbiol Mol Biol Rev. 2005; 69(1):12–50. DOI: 10.1128/MMBR.69.1.12-50.2005 [PubMed: 15755952]
31. Klein AH, Shulla A, Reimann SA, Keating DH, Wolfe AJ. The intracellular concentration of acetyl phosphate in Escherichia coli is sufficient for direct phosphorylation of two-component response regulators. J Bacteriol. 2007; 189(15):5574–5581. DOI: 10.1128/JB.00564-07 [PubMed: 17545286]
32. Castaño-Cerezo S, Pastor JM, Renilla S, Bernal V, Iborra JL, Cánovas M. An insight into the role of phosphotransacetylase (pta) and the acetate/acetyl-CoA node in Escherichia coli. Microb Cell Fact. 2009; 8(1):54.doi: 10.1186/1475-2859-8-54 [PubMed: 19852855]
33. Sadykov MR, Thomas VC, Marshall DD, Wenstrom CJ, Moormeier DE, Widhelm TJ, Nuxoll AS, Powers R, Bayles KW. Inactivation of the Pta-AckA Pathway Causes Cell Death in Staphylococcus aureus. J Bacteriol. 2013; 195(13):3035–3044. DOI: 10.1128/JB.00042-13 [PubMed: 23625849]

34. Wolfe AJ. Physiologically relevant small phosphodonors link metabolism to signal transduction. Current Opinion in Microbiology. 2010; 13(2):204–209. DOI: 10.1016/j.mib.2010.01.002 [PubMed: 20117041]

35. Mizrahi I, Biran D, Ron EZ. Involvement of the Pta-AckA pathway in protein folding and aggregation. Res Microbiol. 2009; 160(1):80–84. DOI: 10.1016/j.resmic.2008.10.007 [PubMed: 19026742]

36. Meier S, Jensen PR, Duus JØ. Real-time detection of central carbon metabolism in living Escherichia coli and its response to perturbations. FEBS Letters. 2011; 585(19):3133–3138. DOI: 10.1016/j.febslet.2011.08.049 [PubMed: 21907715]

37. König C, Simmen HP, Blaser J. Bacterial concentrations in pus and infected peritoneal fluid - implications for bactericidal activity of antibiotics. J Antimicrob Chemother. 1998; 42(2):227–232. [PubMed: 9738841]

38. Kentner D, Martano G, Callon M, Chiquet P, Brodmann M, Burton O, Wahlander A, Nanni P, Delmotte N, Grossmann J, et al. Shigella reroutes host cell central metabolism to obtain high-flux nutrient supply for vigorous intracellular growth. Proc Natl Acad Sci USA. 2014; 111(27):9929–9934. DOI: 10.1073/pnas.1406694111 [PubMed: 24958876]

39. Baba T, Ara T, Hasegawa M, Takai Y, Okumura Y, Baba M, Datsenko KA, Tomita M, Wanner BL, Mori H. Construction of Escherichia coli K-12 in-frame, single-gene knockout mutants: the Keio collection- PubMed - NCBI. Mol Syst Biol. 2006; 2:473.doi: 10.1038/msb4100050

40. Keshari KR, Sriram R, Koelsch BL, Van Criekinge M, Wilson DM, Kurhanewicz J, Wang ZJ. Hyperpolarized 13C-pyruvate magnetic resonance reveals rapid lactate export in metastatic renal cell carcinomas. Cancer Research. 2013; 73(2):529–538. DOI: 10.1158/0008-5472.CAN-12-3461 [PubMed: 23204238]

41. Dahan-Grobgeld E, Livneh Z, Maretzek AF, Polak-Charcon S, Eichenbaum Z, Degani H. Reversible induction of ATP synthesis by DNA damage and repair in Escherichia coli - In vivo NMR studies. J Biol Chem. 1998; 273(46):30232–30238. [PubMed: 9804781]

42. Ezra FS, Lucas DS, Mustacich RV, Russell AF. Phosphorus-31 and carbon-13 nuclear magnetic resonance studies of anaerobic glucose metabolism and lactate transport in Staphylococcus aureus cells. Biochemistry. 1983; 22(16):3841–3849. [PubMed: 6615805]

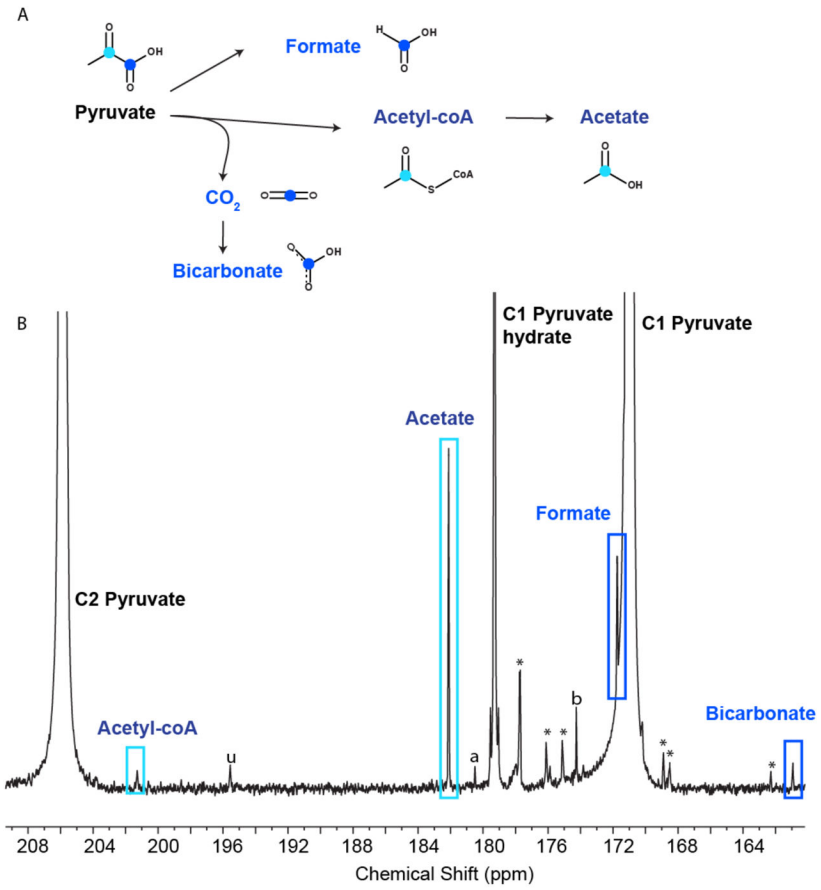

Figure 1. Hyperpolarized pyruvate is metabolized simultaneously by multiple pathways in *E. coli*

A) The schematic of the metabolic fate of the carbons in the first and second position of the pyruvate molecule as its catabolized by *E. coli*. B) ^{13}C hyperpolarized spectrum of the various signals observable upon metabolism of pyruvate by *E. coli*. The * indicates inpurities present in the precursors and the peaks labeled are tentatively identified as: a - βHydroxybutyrate, b-phosphoenolpyruvate. The peak marked ‘u’ is not assigned.

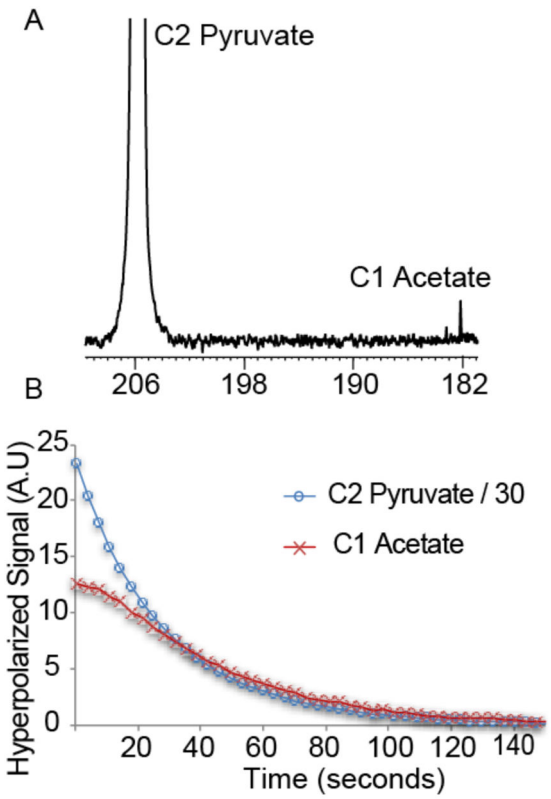

Figure 2. Acetate production is observed from metabolism of hyperpolarized C2 pyruvate in *S. aureus*

A) HP ^{13}C spectra shows the acetate signal that arises from metabolism of C2 pyruvate. B) Kinetics of HP acetate and pyruvate signals show a robust production of acetate.

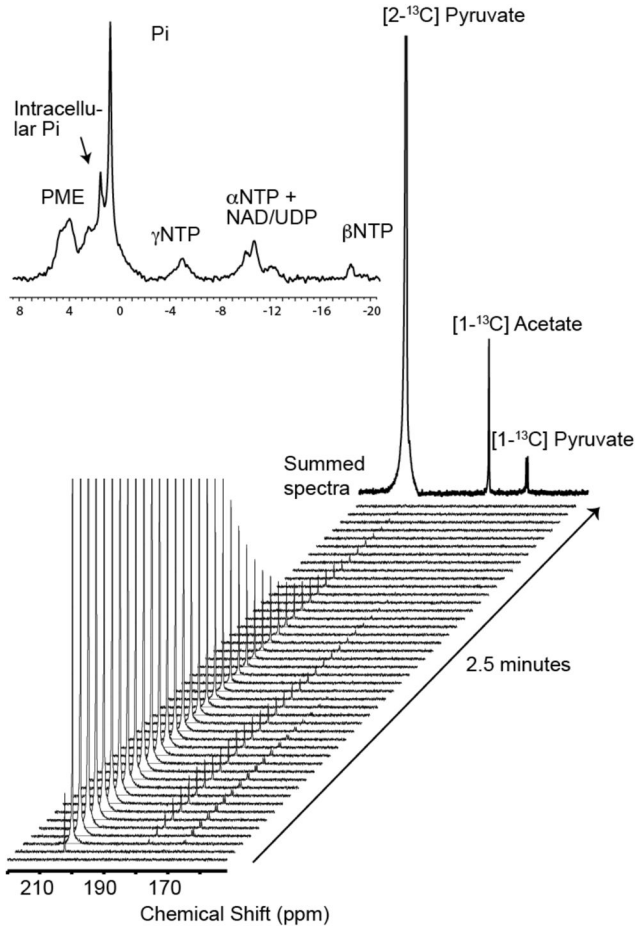

Figure 3. Study of *E. coli* metabolism of HP [2-^{13}C] pyruvate using an NMR-compatible, perfused bioreactor platform

A) ^{31}P spectra of *E. coli* encapsulated in alginate microspheres and shows viable cells. B) [2-^{13}C]pyruvate was injected into the bioreactor and studied for 2.5 minutes seconds. The real-time enzyme kinetics is clearly seen in the production of acetate signal. The summed spectrum at the end reflects the total signal intensity for the entire time course.

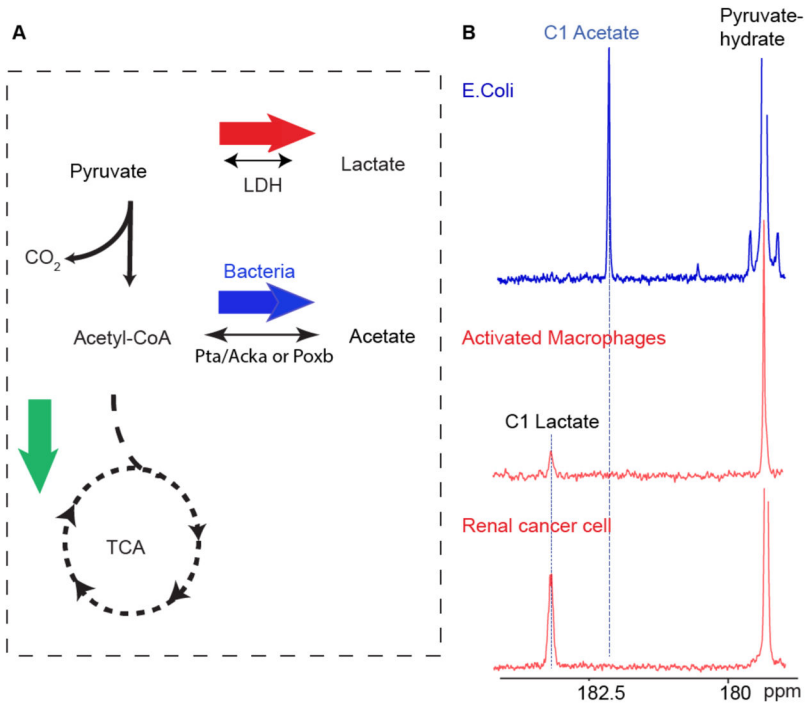

Figure 4. Conversion of [2-^{13}C] pyruvate by bacterial and mammalian cells reveal divergent metabolic pathways

A) Schematic of the bifurcation of pyruvate metabolism that is prevalent in the mammalian cells (green and red arrow) and bacteria (blue arrow). The green arrow denotes the predominant fate of pyruvate in normal functioning mammalian cells. The red arrow denotes the glycolytic phenotype exhibited by most malignant tumors and the blue arrows indicates the primary pathway of wild type bacterial cells. B) C1 and C2 labeled co-polarized pyruvate was injected into mammalian cells or *E. coli*. The top spectrum is that of *E. coli*, a representative gram Gram-negative pathogen. The bacterial cell metabolism clearly depicts the formation of acetate. In contrast, the bottom two spectra corresponding to renal cell cancer and activated macrophages do not have any acetate signal. Furthermore, characteristic mammalian cell metabolism is demonstrated by the lactate signal arising from the C1 pyruvate representative of glycolysis.

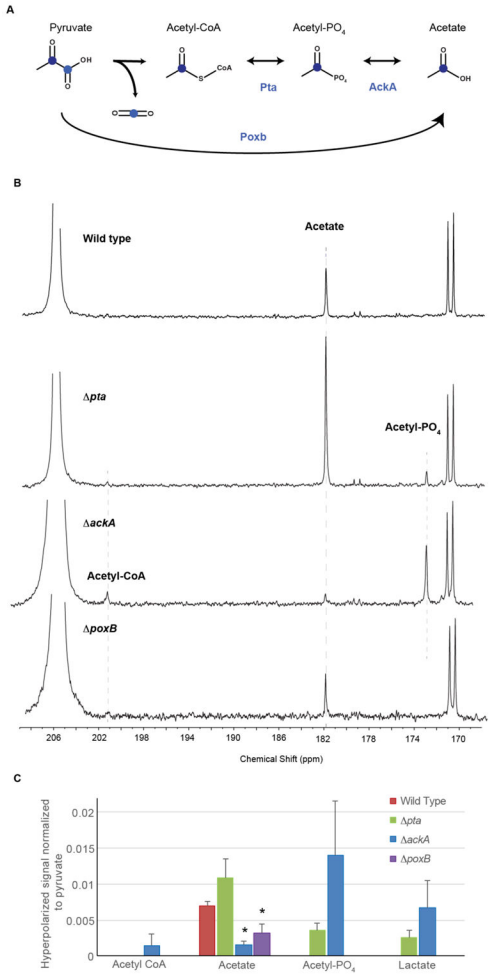

Figure 5. Multiple compensatory pathways of acetate production from pyruvate exists in *E. coli*

A) Schematic of the two major direct pathways of acetate formation from pyruvate. B) Representative spectra for each of the *E. coli* variant depicting the metabolism of hyperpolarized [2-^{13}C] pyruvate. C) Bar graph of the ratios of hyperpolarized metabolites derived from pyruvate in the 4 different *E. coli* cell types studied. The bar graphs represent the mean values of 3 replicates with standard deviation error bars. * denotes statistically significant ($p<0.05$) difference from the wild type *E. coli.*